Journal of Alloys and Compounds 927 (2022) 167048

Contents lists available at ScienceDirect

Journal of Alloys and Compounds

journal homepage: www.elsevier.com/locate/jalcom

Near-infrared rechargeable glass-based composites for green persistent luminescence

N. Garcia Arango[a], S. Vuori[b,c], H. Byron[b,c], D. Van der Heggen[d], P.F. Smet[d], M. Lastusaari[b], L. Petit[a,*]

[a] Photonics Laboratory, Tampere University, Korkeakoulunkatu 3, Tampere 33720, Finland
[b] Department of Chemistry, University of Turku, FI-20014 Turku, Finland
[c] University of Turku Graduate School (UTUGS), Doctoral Programme in Physical and Chemical Sciences, Turku, Finland
[d] LumiLab, Department of Solid State Sciences, Ghent University, Krijgslaan 281-S1, 9000 Gent, Belgium

ARTICLE INFO

Article history:
Received 15 July 2022
Received in revised form 18 August 2022
Accepted 30 August 2022
Available online 5 September 2022

Keywords:
Glass
Glass-ceramic
Tm^{3+} and Yb^{3+} codoping
Luminescence
Up-conversion
Persistent luminescence

ABSTRACT

The fabrication of Yb^{3+}, Tm^{3+} co-doped oxyfluorophosphate glass-based composites, with green persistent luminescence after being charged with near-infrared light, is demonstrated. The mechanism responsible for the green afterglow after near-infrared illumination is unveiled. The composite is prepared using a modified melting process to limit the evaporation of fluorine during melting. Intense (blue and ultraviolet) up-conversion emission is obtained by optimizing the Yb_2O_3 and Tm_2O_3 concentrations. A heat treatment promotes volume precipitation of Yb^{3+}, Tm^{3+} co-doped CaF_2 crystals. Although the intensity of the blue up-conversion emission from the Tm^{3+} $^1G_4$ level is lower in the highly Yb^{3+}-concentrated glass-ceramic due to reverse energy transfer from Tm^{3+} to Yb^{3+}, the heat treatment leads to an increase of the intensity of the emissions around 346 nm, 361 nm nm and 450 nm coming from the Tm^{3+} $^1I_6$ and $^1D_2$ levels. By combining the Yb^{3+} and Tm^{3+} ions with $SrAl_2O_4$:Eu^{2+},Dy^{3+}crystals, green afterglow can be obtained after charging with near-infrared light.

1. Introduction

Luminescent materials are widely applied in solid state lighting, displays, solar energy harvesting, medical imaging or emergency signage [1–3]. They play an important role in the technological transition to more sustainable and energy-saving applications. For decades, there have been efforts to improve the efficiency of these luminescent materials or phosphors. In applications such as white light-emitting diodes where an overlap between the (blue) excitation light and the phosphor's absorption spectrum is ensured by design, this optimization of the overall efficiency mainly comes down to perfecting synthesis procedures, with quantum yields currently almost reaching unity. However, in outdoor applications, for example, the luminescent materials are exposed to sunlight and most of the low energy (red and infrared) light remains unused [4]. One extreme example are glow-in-the-dark materials used in emergency signage or road markings where the situation is even more cumbersome as optically stimulated luminescence by infrared light can potentially lead to a decreased energy storage in the phosphor [5]. In these applications, it is possible to further improve the overall efficiency by converting this low energy (infrared) light to useful high energy (blue) light. The process of converting low energy to high energy photons is called up-conversion. It is usually achieved by exploiting the unique characteristics of the $4f^n$ energy level structure of the rare-earth (RE) elements [6].

RE doped glasses are promising materials for up-conversion (UC) as they are relatively easy to fabricate and at a relatively low cost as compared to single crystals while still having a high transparency in the ultraviolet-visible-near-infrared (UV-Vis-NIR) region. Depending on their compositions, a large amount of RE ions can be incorporated in their amorphous network and as a result, their emission spectra are relatively broad [7]. Phosphate glasses have become materials of interest due to their high RE solubility, [8] their low melting temperature, their high transparency and their relatively high refractive indices compared to silica and silicate glasses, for example [9]. However, their relatively high phonon energies reduce the luminescence quantum efficiency and the excited state lifetime of the RE ions which is detrimental for the upconversion process [10]. On the other hand, fluoride glasses are well-known to have a low phonon energy and thus, when doped with RE, these glasses exhibit intense up-conversion compared to phosphate and silica glasses [11]. However, the processing of fluoride glasses is difficult due to the

* Corresponding author.
E-mail address: laeticia.petit@tuni.fi (L. Petit).

https://doi.org/10.1016/j.jallcom.2022.167048

chemical reactivity of fluoride powders and melts. Additionally, the fluoride glasses have typically relatively low stability with respect to devitrification and have a lower mechanical strength than oxide glasses [12].

Here, as a compromise, an oxyfluorophosphate glass in the $NaPO_3$-CaF_2 system is selected because CaF_2 crystals with low phonon energy were reported to precipitate in the volume of the glass during heat treatment [13]. This is especially interesting considering that the efficiency of the up-conversion process can be greatly enhanced if the RE ions are located in specific crystalline phases instead of in a glassy environment as reported before [14–19]. Indeed, it was demonstrated that a thermal treatment can be used to obtain transparent glass-ceramic from the glass with the 75 $NaPO_3$ – 25 CaF_2 (in mol%). Due to the volume precipitation of Er^{3+} doped CaF_2 crystals, a significant increase in the intensity of green up-conversion is observed after heat treatment confirming that this glass-ceramic is a promising up-converter [20].

By combining luminescent materials such as Yb^{3+} and Tm^{3+} co-doped glasses, which exhibit (UV/blue) up-conversion emission under near-IR excitation, with a persistent phosphor that can be excited by UV/blue light, it becomes possible to prepare a composite that emits visible persistent luminescence (PeL) long after the exposure to near-IR light as shown in Fig. 1 and as demonstrated by Hu et al. [21] in the case of a mixture of upconversion and persistent luminescent particles in polydimethylsiloxane (PDMS).

The addition of the PeL particles to the glass is, however, difficult as the growth of crystals with a specific phase cannot be controlled in glass. Thus, effort has been focused on embedding the phosphor, prepared using alternative synthesis methods with a specific crystalline phase, in amorphous networks; one of the developed techniques being the direct doping method [22].

Herein we describe the fabrication of novel Yb^{3+}, Tm^{3+} codoped glass-based composites containing $SrAl_2O_4$:Eu,Dy particles and exhibiting green afterglow after exposure to infrared light.

2. Material and methods

The Yb^{3+}, Tm^{3+} co-doped glasses with the composition, in mol%: (100-x-y)·(0.75$NaPO_3$-0.25CaF_2)-xYb_2O_3-yTm_2O_3 with x ranging from 0 to 3 and y from 0 to 0.1 (labeled as YbxTmy) were prepared by means of the standard melting-quenching method. The raw materials were $NaPO_3$ (Alfa Aesar, technical grade), CaF_2 (Alfa Aesar, 99.5 %), Yb_2O_3 (Sigma Aldrich, 99.9 %) and Tm_2O_3 (Sigma Aldrich, 99.9 %). The 6 batches were melted in a Pt crucible between 950 and 1000 °C, depending on the composition. After quenching, the glasses were annealed at 40 °C below their respective glass transition temperature for 4 h. After annealing, the glasses were heat treated at (T_g +20 °C) for 17 h followed by 1 h at higher temperature.

The Yb^{3+}, Tm^{3+} co-doped glasses were also prepared with commercial PeL particles with the composition $SrAl_2O_4$:Eu^{2+},Dy^{3+} (Realglow®). After melting the Yb^{3+}, Tm^{3+} co-doped glass, the melting temperature was reduced to a specific temperature, called doping temperature (T_{doping}), prior to adding the PeL particles. Here, 0.5–2 wt% of the PeL particles were added into the glass melt at T_{doping} ranging from 875 to 950 °C. The dwell time between the addition of PeL particles in the glass melt and the quenching step was 3 min. After quenching, the glasses were annealed at 40 °C below their respective glass transition temperature for 4 h.

Scanning Electron Microscopy (SEM) analysis was performed using Carl Zeiss Crossbeam 540 Gemini SEM with an Energy Dispersive X-ray Spectroscopy (X-MaxN 80) detector (EDS). Samples were polished and coated with a conductive carbon layer to improve the outcome of the measurement. Fluorine in the glasses was quantified using an Electron Probe MicroAnalyzer (EPMA) coupled with a wavelength dispersive X-ray analyzer (WDX). The accuracy is ± 0.1 at%. Scanning transmission electron microscopy (STEM) was performed using a JEOL F200 S/TEM with acceleration voltage of 200 kV. The energy-dispersive X-ray spectroscopy (EDS) was carried out using the integrated Jeol Dual EDS system. After polishing, the samples were prepared by depositing on copper holey carbon grid a droplet of a solution made of the glasses crushed into powder dispersed in ethanol.

The thermal properties of the glasses were determined using a NETZSCH STA 449 F1 Differential Scanning Calorimeter (DSC), with a heating rate of 10 °C/min, resulting in an accuracy of approximately ± 3 °C. The glass transition temperature (T_g) was taken as the inflection point of the first endothermic signal and the crystallization temperature (T_p) at the exothermic peak maximum. The onset of crystallization (T_x) was obtained as the intersection of the tangent of the exotherm peak with the baseline.

The density was measured considering the Archimedes principle with the OHAUS Adventurer Analytical Scale device, and an uncertainty of around ± 0.02 g/cm^3.

The IR spectra of the samples were obtained using PerkinElmer Spectrum One FTIR2000 Spectrometer (Waltham, MA, USA) including the Attenuated Total Reflectance (ATR) mode. The range of the measurement was from 600 cm $^{-1}$ to 1600 cm^{-1} and the spectra were normalized to the band centered around 900 cm^{-1}, with an accuracy of approximately 2 cm^{-1}.

X-ray diffraction study was performed to identify the crystalline phases precipitating in the glasses during heat treatment using a Panalytical EMPYREAN multipurpose X-Ray Diffractometer (XRD), for the measurement, a Ni filtered Cu-Kα radiation is used and the diffractogram is obtained from 2θ = 15–80°, having a step of 0.013°.

The absorption and transmission spectra, measured using polished samples from a range of 200–1500 nm, were recorded using a UV–VIS–Near-IR Spectrophotometer (UV-3600 Plus, Shimadzu). The absorption-cross sections were calculated using Eq. (1).

$$\sigma_{abs}(\lambda) = \frac{\ln 10 \quad \log\left(\frac{I}{I_0}\right)}{NL} \tag{1}$$

where N is the concentration of RE ions per cm^3, L the thickness of the glass (cm) and $\log\left(\frac{I}{I_0}\right)$ the absorbance. The accuracy is ± 10%.

The up-conversion spectra of the glasses were recorded using a TEC-cooled fiber-coupled multimode laser (II-VI Laser enterprise), with $\lambda_{exc} \sim 980$ nm, reaching the surface with a power of approximately 400 mW. The emission spectra were later recorded in a range of 400–700 nm by means of a Spectro 320 optical spectrum analyzer (Instrument Systems Optische Messtechnik GmbH, Germany). The emission spectra in the 900 – 1700 nm range were obtained using a Ti-sapphire ring laser (0.4 cm^{-1} linewidth) as exciting light and an extended IR Hamamatsu H10330A-75 photomultiplier and finally amplified by a standard lock-in technique. The emission spectra in the 280–820 nm range were measured using a ProEM 1600 EMCCD camera attached to an Acton SP2300 monochromator (Princeton Instruments) which was intensity calibrated using a S401C thermal power sensor coupled to a PM400 read-out console (Thorlabs Inc.). All emissions were obtained at room temperature.

The PeL spectra of the $SrAl_2O_4$:Eu^{2+},Dy^{3+} containing glasses were measured at room temperature using a Varian Cary Eclipse Fluorescence Spectrophotometer equipped with a Hamamatsu R928 photomultiplier (PMT). The samples were irradiated for 5 min at room temperature with a compact UV lamp (UVGL-25, 4 W, λ_{exc}: 254 nm) and the PeL spectra were collected 1 min after stopping the irradiation. When using 980 nm charging, the samples were first irradiated for 5 min at room temperature with a 980 nm laser module operated at 6000 mA and then the PeL spectra were recorded 15 s after stopping the irradiation. For the PeL decay curve measurements, the samples were irradiated for 5 min with a 254 nm hand-held UV-lamp (UVGL-25). The luminance curves were obtained by measuring the luminance every second starting 5 s after

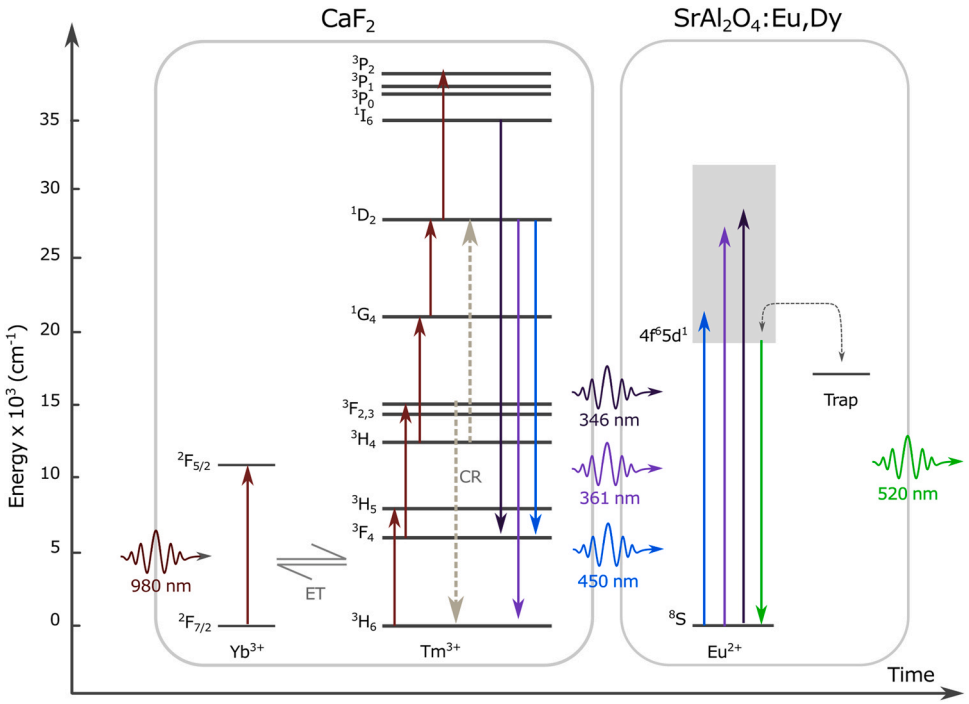

Fig. 1. Schematic representation of the different luminescence processes that lead to the emission of green afterglow after exposure of the composite to 980 nm infrared light. Note that only some upconversion pathways are shown. Also cross-relaxation (CR) and collaborative energy transfer processes can take place.

stopping the excitation using a Hagner ERP-105 luminance meter coupled with a Hagner SD 27 detector. The PeL decay after illumination by a 200 mW, 980 nm laser focused on 0.25 mm², was measured using an ILT 1700 calibrated photometer (International Light Technologies) equipped with a photopic filter (YPM). For these measurements, a metal plate with a circular hole (Ø 5 mm) was inserted between the sample and the detector in order to maximally exclude effects due to differences in sample size and morphology. For the experiment to demonstrate that trapping and afterglow are induced by the up-conversion process, the samples were illuminated with a 200 mW, 980 nm laser focussed on 0.25 mm². Afterglow emission spectra were recorded using the ProEM1600 EMCCD camera attached to the Acton SP2300 monochromator. Integration over the emission band resulted in the afterglow emission intensity.

3. Results and discussion

In this study, oxyfluorophosphate glasses are prepared with different concentrations of Tm^{3+} and Yb^{3+} to develop a glass with intense blue UC emission. In Table 1, the physical and thermal properties of some of the glasses are listed.

An increase in the content of Tm^{3+} and Yb^{3+} increases the density (ρ) and the thermal properties of the glasses. The changes in the density with an increase in the concentration of the RE ions are due to the heavy Yb and Tm which replace the other elements, while the rise in the glass transition temperature (T_g) can be related to an increase in the strength of the glass network. An increase in the concentration of Tm^{3+} and Yb^3 increases also the temperatures related to crystallization (T_x and T_p), and also ΔT (T_x-T_g) indicating a better resistance of the glass against crystallization from the highly RE concentrated glasses [23]. Similar enhancement of the thermal stability by RE addition was reported in [24].

The structure of the glass is investigated using IR spectroscopy. The IR spectra of the investigated glasses are similar to those reported in [25,26] (Fig. 2).

The glass structure is thought to be formed by Q^2 and Q^1 units, 2 and 1 being the number of bridging oxygens per tetrahedron, respectively. The progressive introduction of Yb^{3+} ions leads to a depolymerization of the phosphate network which can be described as a decrease in the Q^2 units associated with an increase in the Q^1 units. This change in the glass structure is evidenced by the decrease in intensity of the bands at 650–800, 850–1050, 1080 and 1250 cm^{-1} (bands associated with Q^2 units, especially ν_s(P – O–P), ν_{as}(P-O-P), ν_s (P – O–P) and ν_{as}(O-P-O), respectively [27]) and the increase of the band at 1130 cm^{-1} (the band associated with asymmetric stretching vibrations of the PO_3^{2-} in Q^1 units [28]) compared to the band at 880 cm^{-1}. The increase in the Q^1 units, associated with a decrease in the rings in the Q^2 units, is confirmed by the rise in intensity of the shoulders at ~960 and 1020 cm^{-1} (associated with the asymmetric stretching vibration in small and large rings, respectively in Q^2 units, respectively) and of the shoulders at ~980 and 1085 cm^{-1} (related to the symmetric and asymmetric stretching vibration of PO_3^{2-} units in Q^1 units, respectively) [29]. The increase in T_g indicates that the depolymerization of the phosphate network induced by the addition

Table 1
Thermal and physical properties of the glasses prepared with different amount of Tm^{3+} and Yb^{3+}.

Glass	Yb^{3+} ions/cm^3 (10^{20})	Tm^{3+} ions/cm^3 (10^{19})	T_g ± 3 (°C)	T_x ± 3 (°C)	ΔT (T_x-T_g) ± 6 (°C)	T_p ± 3 (°C)	ρ ± 0.02 (g/cm^3)
Yb 0 Tm 0	0	0	268	326	58	345	2.57
Yb 1 Tm 0.05	3.21	1.60	285	360	75	380	2.64
Yb 2 Tm 0.05	6.49	1.62	294	380	86	437	2.75
Yb 3 Tm 0.025	9.81	0.82	304	426	122	534	2.85
Yb 3 Tm 0.05	9.76	1.63	303	443	140	520	2.84
Yb 3 Tm 0.1	9.82	3.27	303	378	75	399	2.86

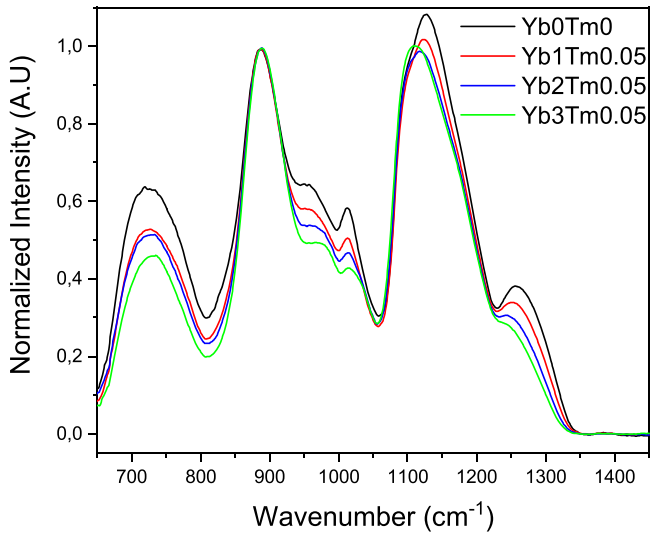

Fig. 2. Normalized IR spectra of undoped glass (Yb0Tm0) and the glasses prepared with 0.05 mol% of Tm_2O_3 and different concentrations of Yb_2O_3.

of rare-earth ions leads to the replacement of the P-O-P bonds by P-O-M (M=Yb, Tm) bonds as suggested in [30].

The incorporation of the RE in the glasses is further evidenced by their absorption spectra which show the absorption bands characteristic for Yb^{3+} and Tm^{3+}, although the former has a much lower intensity due to its small concentration (Fig. 3a). The spectra clearly exhibit the typical $^2F_{7/2} \rightarrow {}^2F_{5/2}$ absorption band of Yb^{3+} in the 850–1050 nm range which is important for the upconversion mechanism. The intensity of this band grows with an increase in the Yb_2O_3 content (Fig. 3b). The absorption cross-section at 980 nm measured at (1.11 ± 0.06) x 10^{-21} cm^{-2} is independent of the glass composition and is similar to the absorption cross-section of other Yb^{3+}-doped phosphate glasses [31].

Blue up-conversion (UC) is achieved from the glasses at room temperature after 980 nm excitation. The UC spectra exhibit bands at 475 and 650 nm due to the $^1G_4 \rightarrow {}^3H_6$ and $^1G_4 \rightarrow {}^3F_4$ transitions of Tm^{3+}, respectively (Fig. 4a).

As depicted in Fig. 4b, the progressive addition of Tm^{3+} ions reduces the intensity of the emission centered at 475 nm due to concentration quenching and so probably due to shorter distances between Tm^{3+} ions favoring the cross-relaxation mechanism as reported in [32]. However, the blue UC is greatly enhanced by increasing the Yb^{3+} content, confirming that Yb^{3+} ions act as sensitizers. As presented in Fig. 1, the absorption of the 980 nm photon excites the Yb^{3+} ions at the ground state to the $^2F_{5/2}$ state, from which the energy is transferred to Tm^{3+} ions which are then excited to the $^3H_5$ state relaxing to the $^3F_4$ state by non-radiative transition. The second energy transfer between Yb^{3+} and Tm^{3+} can excite the Tm^{3+} ions to the $^3F_{2,3}$ state which populates the $^3H_4$ state. The third process excites the Tm^{3+} ions populating the $^1G_4$ state.

Different pump power densities are used to collect the UC spectra to explain the blue UC process occurring in the newly developed glasses. The changes in the UC emission intensity with the pump power density are connected to the number of photons (n) involved in the UC process as I_{em} is about $(P_{pump})^n$. The slope of the logarithmic plot of the blue (475 nm, $^1G_4 \rightarrow {}^3H_6$) UC intensity as a function of the pump power laser density is ~ 2.66 for all glasses, independently of their compositions (Fig. 5a) confirming that the $^1G_4 \rightarrow {}^3H_6$ UC emission is related to the three-photon process in all the investigated glasses.

As presented in Fig. 5b, in addition to the emission bands from Tm^{3+} at ~1450 and 1650 nm due to the $^3H_4 \rightarrow {}^3F_4$ and $^3F_4 \rightarrow {}^3H_6$ transitions, respectively, an emission at ~1000 nm can be seen when pumping the glasses at 791 nm. This emission at 1000 nm can be assigned to the Yb^{3+} $^2F_{5/2} \rightarrow {}^2F_{7/2}$ emission, indicating that energy transfer from Tm^{3+} to Yb^{3+} also takes place in the glasses due to a non-resonant phonon-assisted energy transfer between both ions [33]. The emission at 1000 nm is due to the energy transfer from the level $^3H_4$ of Tm^{3+} to the $^2F_{5/2}$ state of Yb^{3+}. One should mention that no UC is observed when using 791 nm pumping due to the low concentration of Tm_2O_3 in the glasses.

Since an enhancement of the UC properties was reported after a thermal treatment of Er^{3+}-doped glasses in similar glass systems due to the volume precipitation of Er^{3+}-doped CaF_2 crystals occurring during heat treatment [25,26], the glasses were heat treated for 17 h at (T_g+20 °C) and then at their respective T_p for 1 h in order to check if a heat treatment of the investigated Yb^{3+}, Tm^{3+} co-doped glasses can also be applied to enhance their UC properties. After heat treatment, the glasses are translucent with no noticeable sign of surface crystallization in agreement with the loss in the transmittance of the glasses after heat treatment (see Fig. 6a).

The crystallization of the glass due to the thermal treatment is confirmed using XRD. The presence of the three peaks located at 2θ = 33°, 55.2°and 65.8° in the XRD pattern of the heat treated Yb1 glasses confirms the precipitation of CaF_2 (ICDD 00–035–0816)

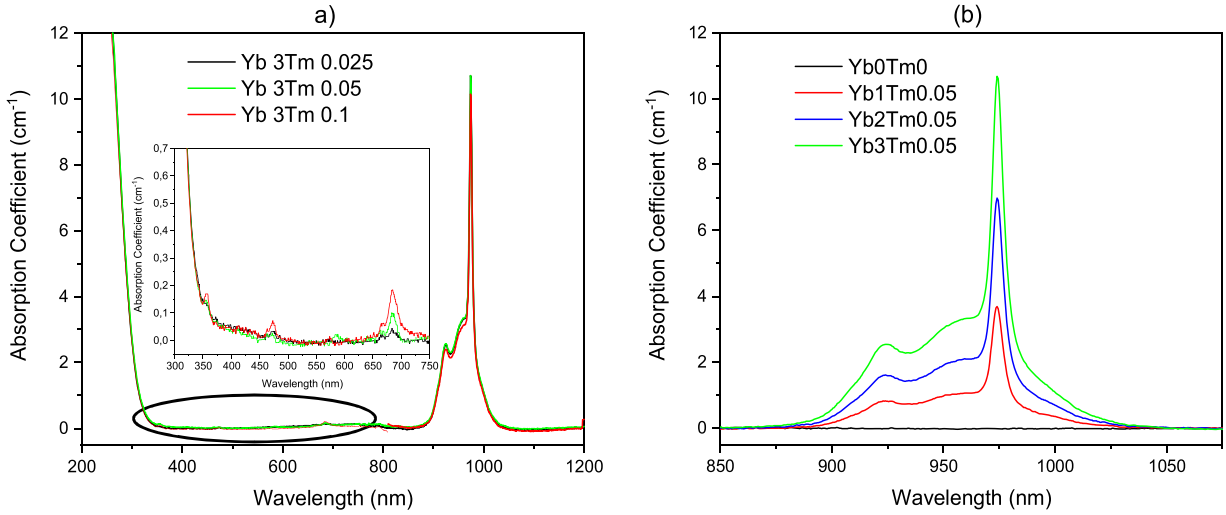

Fig. 3. Absorption spectra of the glasses prepared with different concentration of (a) Yb_2O_3 and of (b) Tm_2O_3.

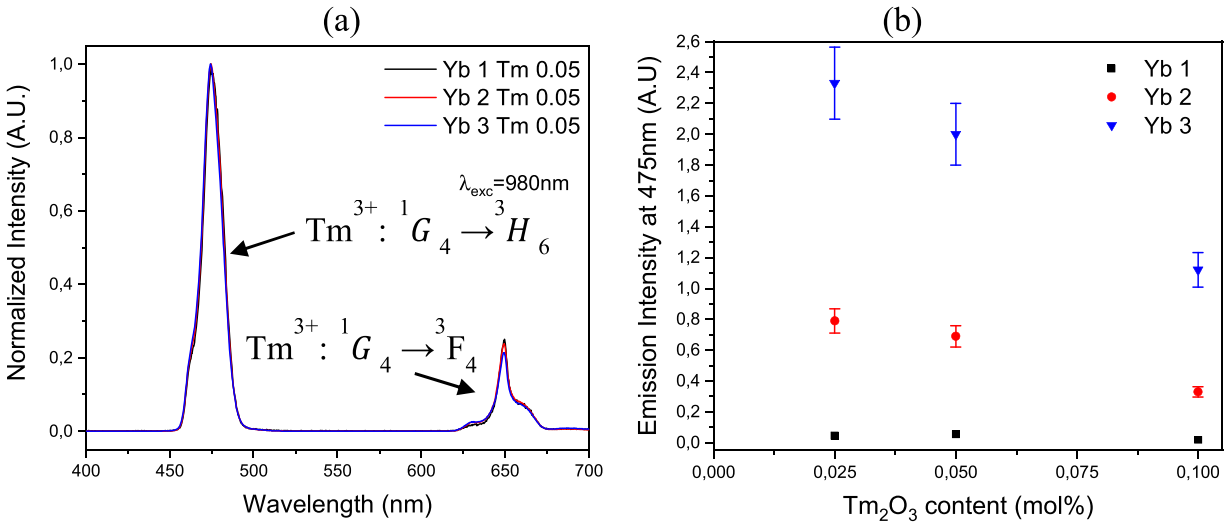

Fig. 4. (a) Normalized UC spectra of some glasses, taken as examples, obtained under 980 nm excitation, (b) Intensity of the emission at 475 nm under 980 nm excitation as a function of the Tm_2O_3 content.

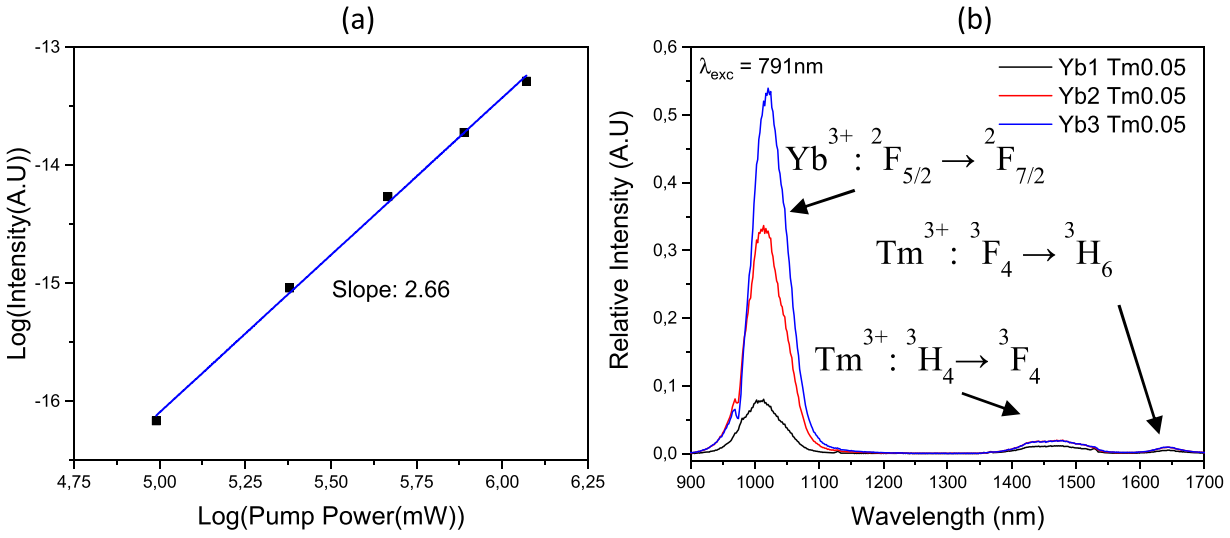

Fig. 5. (a) Dependence of the blue emission intensity monitored at 475 nm on the excitation power density for the glass Yb3Tm0.05 taken as an example, (b) Emission spectra of the glasses prepared with 0.05 mol% of Tm_2O_3 and different concentrations of Yb_2O_3 under excitation at 791 nm.

crystals in these glasses (Fig. 6b). However, other crystals such as $NaPO_3$ (ICDD 04–011–3120) and $Na_2Ca_2P_2O_7F_2$ (ICDD 04–012–1844) are present in the Yb2 and Yb3 glasses when heat treated at (T_g +20 °C) for 17 h and then at T_p for 1 h. Similar crystals were reported to precipitate in Er^{3+} doped glasses during heat treatment [25,26]. It is the presence of these additional crystals which is thought to reduce the transparency of the Yb2 and Yb3 glasses compared to the Yb1 glass after heat treatment (Fig. 6a). According to [25,26], the growth of the $NaPO_3$ and $Na_2Ca_2P_2O_7F_2$ crystals at the expense of CaF_2 crystal can be related to the high temperature used during the crystal growth step. Thus, when the crystal growth step is performed at 390 °C instead of the T_p of each glass, only the peaks related to CaF_2 crystals can be seen in the XRD pattern of the heat treated Yb2 and Yb3 glasses (Fig. 6b). The transmittance spectra of these glasses were found to be similar to that of the heat treated Yb1 glass (Fig. 6a). The mean size of the crystallites is estimated using the Scherrer's equation as in [26] and is estimated to be 16 nm in the Yb1 glass-ceramics, similar to the one reported in Er^{3+} doped glass in the same glass system [26,34]. The mean size of the crystallites increases slightly to ~24 nm when the concentration of Yb_2O_3 increases to 3 mol%. The increase in the Tm_2O_3 content from 0.025 to 0.1 mol% is too insignificant to have a noticeable impact on the mean size of the crystallites. The increase in the mean size of the crystallites with the progressive addition of RE reveals that the dopants have an impact on the crystal growth as reported for other glass-ceramics [35]. In agreement with [36], the crystallization activation energy is expected to decrease with increasing the doping level.

The presence of Yb^{3+} and Tm^{3+} in the CaF_2 crystals in the glasses is evidenced using TEM coupled with EDX (Fig. 6c). According to the composition analysis, the crystals contain Yb and Tm which is also supported by the changes in the emission line shape of the Tm^{3+} and Yb^{3+} under 980 or 791 nm excitation (Figs. 7a and 7b).

As depicted in Fig. 8a, the intensity of the $^1G_4 \rightarrow {}^{3H}_{6}$ UC emission of the Yb1 glasses is stronger after heat treatment due to the presence

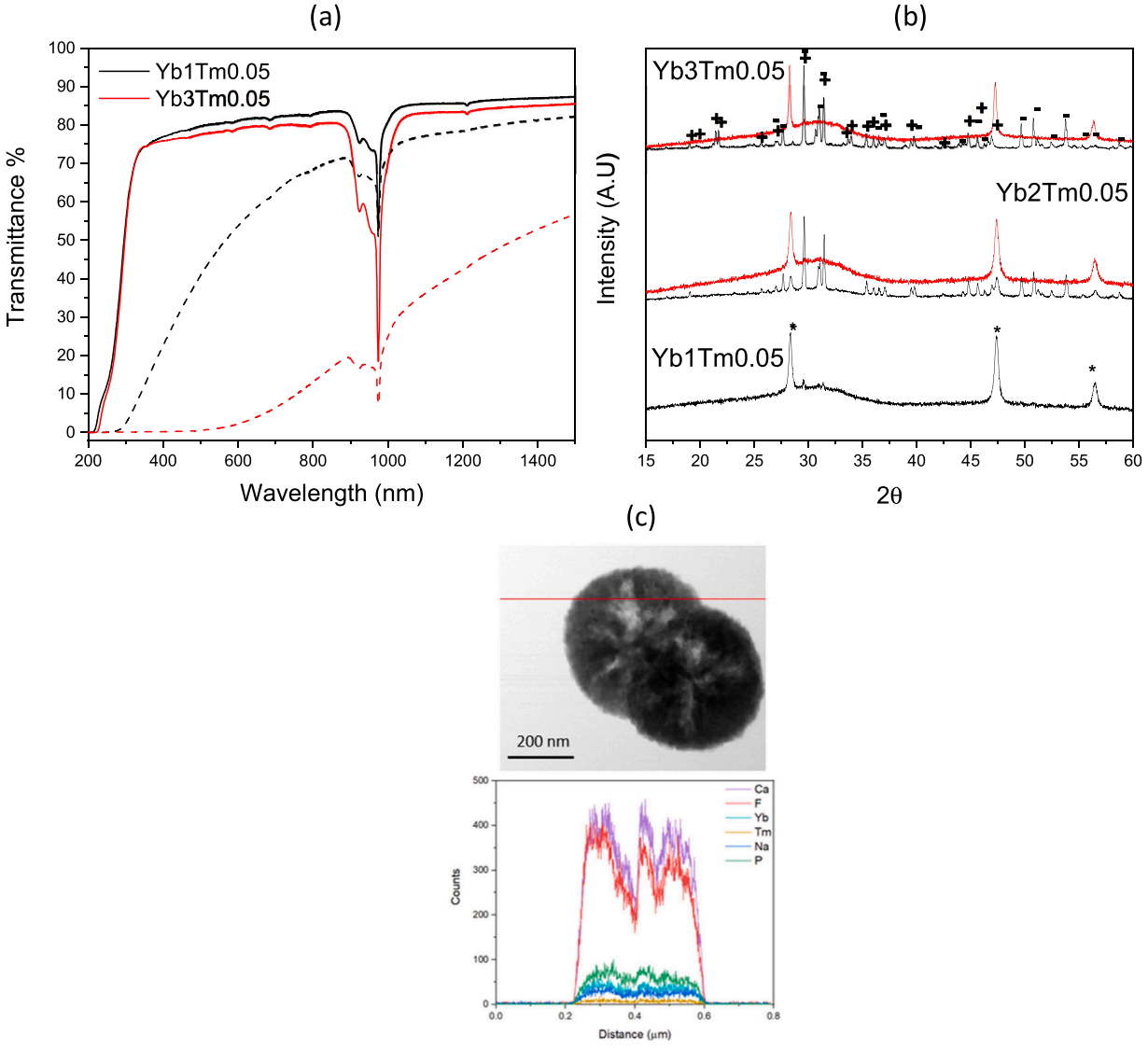

Fig. 6. (a) Transmittance spectra of some glasses, taken as examples, prior to (solid line) and after heat treatment at their respective (T_g+20 °C) for 17 h and then at T_p for 1 h (dashed lines). Sample thickness is 1.3 mm. (b) XRD pattern of the glasses heat treated at their respective (T_g+20 °C) for 17 h and then at T_p for 1 h (black) and at their respective (T_g +20 °C) for 17 h and then at 390 °C for 1 h (red) [Peaks correspond to * CaF_2, +$NaPO_3$, - $Na_2Ca_2(P_2O_7)F_2$], (c) TEM micrograph with corresponding composition analysis of Yb1Tm0.05 glass after heat treatment at (T_g+20 °C) for 17 h and then at 390 °C for 1 h.

of Yb^{3+} and Tm^{3+} in the crystals with high crystal symmetry and low phonon energy. However, the intensity of this UC emission decreases after heat treatment of the Yb2 and Yb3 glasses (Fig. 8b and c). As the Yb_2O_3 content increases, the distance between the Yb^{3+} ions in the CaF_2 crystals is reduced to the point that reverse energy transfer processes from the activator to the sensitizer become dominant, as evidenced by the increase in intensity of the Yb^{3+} emission under 791 nm excitation (Fig. 7b). This is in agreement with a recent study in which 1.5 mol% of Yb_2O_3 was reported to yield the largest up-conversion improvement in glass-ceramics containing Yb^{3+}, Pr^{3+} co-doped CaF_2 crystals [37].

It should be pointed out that the intensity of the $^1_4{}^G \rightarrow {}^3H_6$ UC emission depends on the temperature used for the crystal growth step and thus on the amount of CaF_2 crystals precipitating in the glass; the higher the growth temperature, the lower the amount of CaF_2 crystals and thus the lower the intensity of the UC emission.

When adding the PeL particles in glasses with blue upconversion, it is important to maximize the amount of UC emission that can be used to excite the PeL particles. The thermoluminescence excitation spectrum (also called the trap filling spectrum) of $SrAl_2O_4$:Eu,Dy is shown in Fig. 9. Also shown are the UC spectra of the as prepared and heat treated Yb3Tm0.05 glasses observed under excitation with 980 nm light. Especially, the spectra exhibit emissions around 346, 361 and 450 nm which correspond to the $^1I_6 \rightarrow {}^3F_4$, $^1D_2 \rightarrow {}^3H_6$ and $^1D_2 \rightarrow {}^3F_4$ transitions of Tm^{3+}, respectively, in addition to the emission at 475 nm. After the heat treatment, the samples exhibit enhanced UC emission with respect to the emission at 475 nm, especially at 346 nm (originating from $^1I_6$) and to a lesser extent for the emission at 361 nm and 450 nm (originating from $^1D_2$), indicating that the heat treatment increases the relative probability of stacking more than three photons most likely due to reduced non-radiative pathways or due to a better coupling between the Yb and

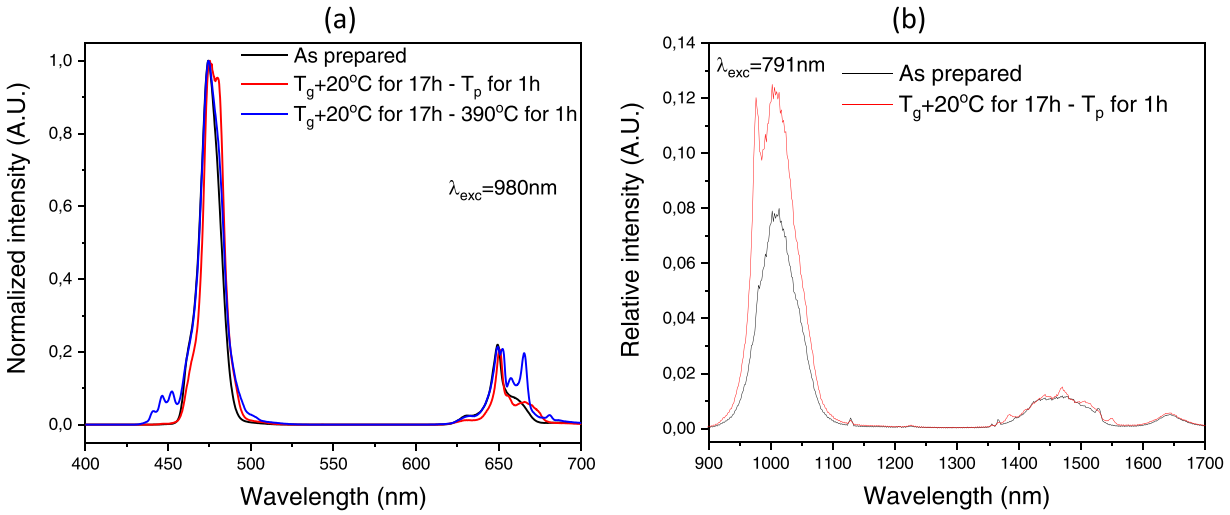

Fig. 7. (a) Normalized UC spectra of Yb3Tm0.05 glasses prior to and after heat treatment obtained under 980 nm excitation; (b) Emission spectra of the Yb1Tm0.05 glass prior to and after heat treatment obtained under 791 nm excitation.

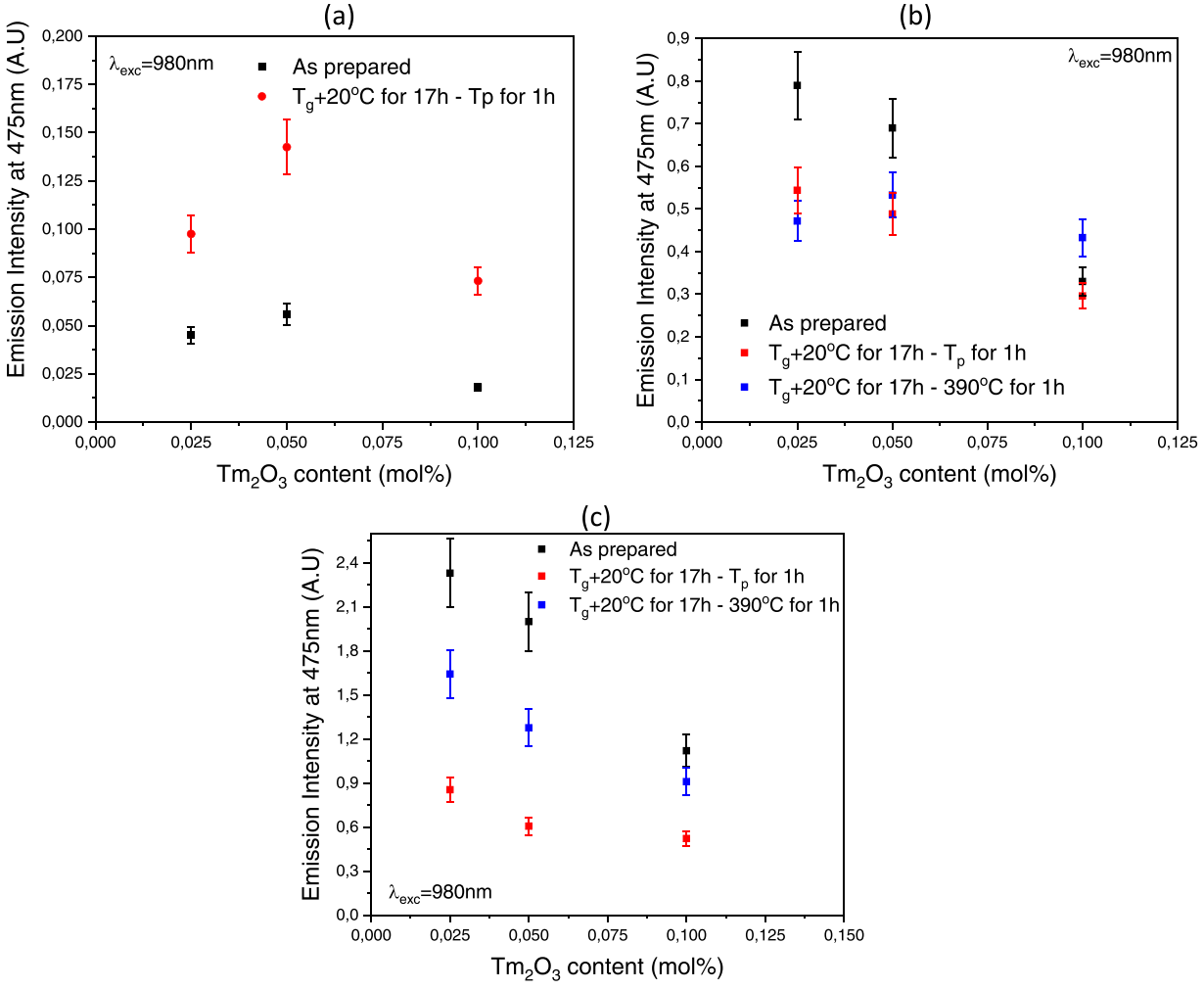

Fig. 8. Intensity of the emission at 475 nm under 980 nm excitation of the Yb1 (a), Yb2 (b) and Yb3 (c) glasses prior to and after heat treatment.

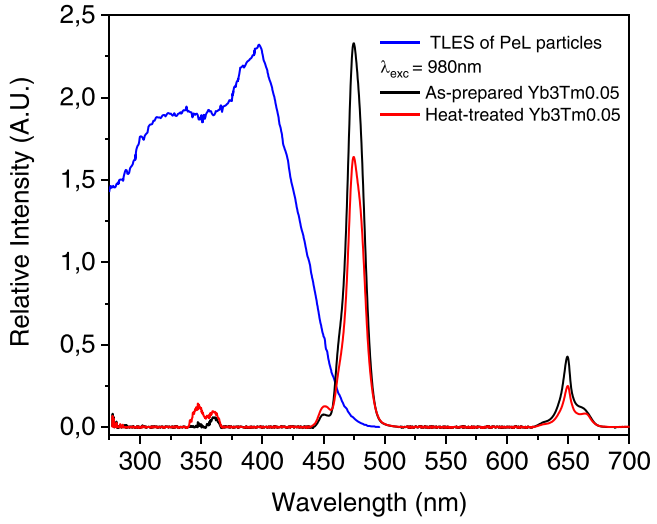

Fig. 9. UC emission spectra of the Yb3Tm0.05 glass prior to and after heat treatment and thermoluminescence excitation spectrum (TLES) of the PeL particles, taken from [39].

Tm ions after the heat treatment. This would be in agreement with Chen et al. who observed a slope of 3.8 in the power dependency plot for the emission peaks originating from the $^1D_2$ level (361 nm, 450 nm) and 4.5 for the 346 nm emission transition, starting at $^1I_6$ [38].

It is clear that the overlap between the thermoluminescence excitation spectrum of the PeL particles and the UC spectrum of the Yb3 glass-based materials is the highest for the 345, 361 and 450 nm emissions while it is only limited for the 475 nm emission from the $^1G_4$ level. Consequently, despite the relative loss in the emission at 475 nm after heat treatment of the Yb3Tm0.05 glass, the emergence of the 346, 361 and 450 nm upconversion emission bands suggests that it might be easier to excite the PeL particles after the heat treatment.

The PeL particles (0.5 wt%) were incorporated into the Yb3Tm0.05 glass using the direct doping method where the PeL particles are introduced in the glass melt after the melting and prior to the quenching. As explained in [40–43], corrosion of the PeL particles, associated with a loss in the PeL properties, always occurs during this process. The level of the decomposition depends on the doping parameters: the temperature at which the particles are added (T_{doping}) and also the duration the PeL particles are in the glass melt prior to the quenching (dwell time). It should be also noted that the preparation of these oxyfluoride glasses is challenging due to fluorine which is a volatile element as discussed in [44]. To limit the evaporation of fluorine, the dwell time was set to 3 min, as opposed to the 5 min dwell time which is usually employed to prepare oxide glasses [42]. The T_{doping} was varied between 875 and 950 °C, the melt being too viscous to be poured when using lower temperature than 875 °C whereas 950 °C is below the melting temperature (1000 °C). The picture of the glasses is shown in Fig. 10a.

Green PeL can be seen from all the glasses after being charged with UV light at 254 nm, confirming the (at least partial) survival of the PeL particles during the melting process. However, the intensity of the green PeL decreases as the T_{doping} increases, as reported in Refs [40–43]. Indeed, as the T_{doping} increases, the PeL particles degrade inside the glasses, losing their PeL properties. As suggested in [45], the decomposition of the PeL particles can be evidenced by the appearance of an Al rich outermost region in the PeL particles as seen Fig. 10b. The amount of Al in this layer increases as the T_{doping} increases confirming the progressive corrosion of the PeL particles while embedding them in the glass using high T_{doping}. P- and Yb-rich crystals can also be seen at the particle-glass interface. As more crystals can be seen in the glasses prepared with high T_{doping}, it is possible that the precipitation of these crystals occurs due to the decomposition of the PeL particles and so due to the diffusion of Al and Sr into the glasses. The PeL particles are expected to behave as a nucleation agent leading to heterogeneous nucleation. Still, one should mention that these P- and Yb-rich crystals cannot be seen in the XRD analysis, implying that their concentration remains low in the glass matrix.

Although partial decomposition of the PeL particles happens during the glass melting leading to Al and Sr diffusion into the glass matrix, no changes in the shape of the UC emission spectrum were seen, indicating that the sites of Yb^{3+} and Tm^{3+} remain unchanged after adding the PeL particles in the glass. However, the intensity of the UC emission at 475 nm from the PeL glasses is lower compared to that of the PeL free glasses (Fig. 10c). While this can be related to the partial overlap of the UC emission at 475 nm with the absorption spectrum of the PeL particles, the decrease in the intensity of the blue emission can also be related to the increase in the T_{doping} as recently reported in [46]. Indeed, as the T_{doping} increases, the amount of fluorine in the glass decreases as confirmed using EPMA reducing the intensity of the blue UC emission (Fig. 10c). This means that shortening the dwell time to 3 min does not sufficiently restrict the evaporation of fluorine during the glass preparation and so the direct doping method was modified accordingly: the PeL particles were added after melting at 1000 °C and the glass was quenched after adding the PeL particles. Due to the shorter melting process as compared to the direct doping method, it is possible to produce a PeL glass with a similar amount of F and thus similar intensity of blue UC emission as the glass prepared using low T_{doping} (Fig. 10c). As shown in Fig. 10a, the glass exhibits homogeneous and intense green afterglow after illumination with UV light at 254 nm. As presented in Fig. 10b, no Al rich layer is observed at the particle-glass interface, confirming that the addition of the PeL particles before the quenching limits not only the evaporation of fluorine but also the decomposition of the PeL particles.

As the modified direct doping method permits the production of oxyfluoride glass with limited losses in fluorine while preventing, in the same time, the decomposition of PeL particles, Yb3Tm0.05 glasses are prepared with different amount of PeL particles. One should be pointed out that 2 wt% is the maximum of PeL particles which could be added in the glass melt without increasing significantly the viscosity of the glass melt. All glasses exhibit homogenous green afterglow, the intensity of which increases with the wt % of the PeL particles (Fig. 11a).

The addition of more than 1 wt% of PeL particles leads to crystallization during quenching, confirming the role of the PeL particles in the heterogeneous nucleation process. The large amount of crystals precipitating in the glass matrix are clearly seen in the SEM image of the glass prepared with 2 wt% of PeL particles (Fig. 11b).

When charging the glasses with 980 nm for 5 min, green afterglow can be seen from all the glasses (Fig. 12a), the intensity of which increases with the amount of PeL particles. This green afterglow after charging with 980 nm light can be understood when considering the overlap between the UC emission and the thermoluminescence excitation spectrum of $SrAl_2O_4$:Eu,Dy (Fig. 9) [47] indicating that the PeL particles are not directly excited by infrared light but by the blue light resulting from the UC process. The occurrence of emission in phosphors after stimulation with infrared light is, however, usually a consequence of an optically stimulated de-trapping process, which is often followed directly by radiative recombination at the activator in a process that is called optically stimulated luminescence (OSL) [48,49]. Alternatively, in some phosphors, stimulation with infrared light transfers charges from one trap to another [50,51]. Since it is known that $SrAl_2O_4$:Eu,Dy has a very deep trap [52], it is not unlikely that infrared stimulation

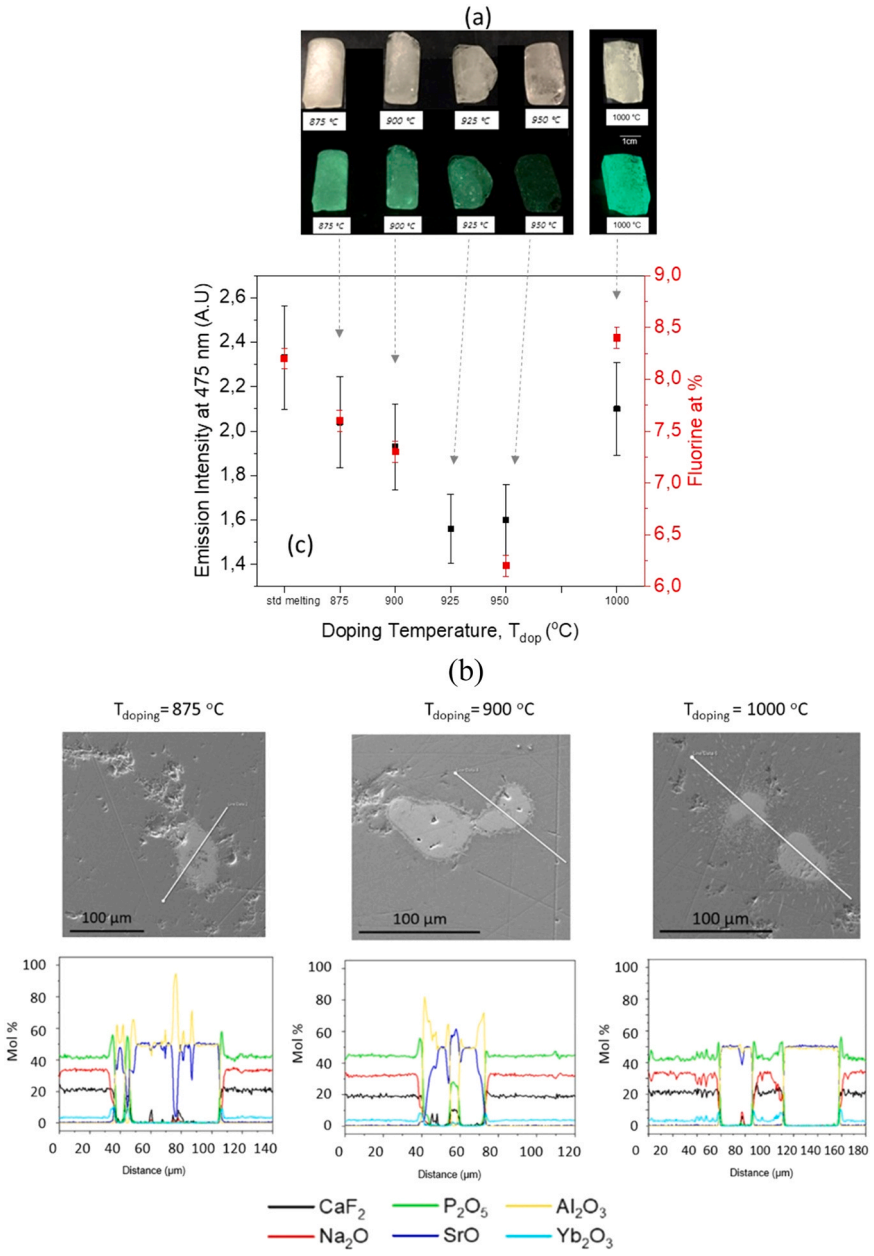

Fig. 10. (a) Picture in daylight and after stopping the UV excitation of the Yb3Tm0.05 glasses prepared using different T_{doping} and of the glass prepared when adding the PeL particles in the glass melt at 1000 °C before the quenching. (b) SEM images with corresponding composition analysis of a PeL particle found at the surface of the polished Yb3Tm0.05 glasses prepared using different T_{doping}; (c) Intensity of the emission at 475 nm (λ_{exc} = 980 nm) and the fluorine content as a function of different T_{doping}.

could induce a transfer of trapped charges from this deep trap to shallower traps resulting in an increased afterglow intensity after 980 nm illumination. To unambiguously determine the mechanism responsible for the green afterglow after IR illumination, the response of an undoped (Yb0Tm0) glass containing only PeL particles was compared to that of a doped glass containing the same wt% of PeL particles. The results are shown in Fig. 12b from which it is clear that only the doped glass exhibits afterglow after 980 nm illumination, confirming that the phosphor is effectively charged by the blue UC light and that other mechanisms related to OSL or deep traps can be ruled out. One should note that during the experiments, this irradiation time was evaluated and 2 min was sufficient to reach saturation, so no longer times were needed.

When charged with 254 nm UV (6 mW/cm^2 irradiance) for 5 min, the glass with 2 wt% of PeL particles emits green light for 100 min above the 0.3 mcd/m^2 limit set in the exit signage standards [53] as the limit of visibility (Fig. 13a). The afterglow decay curves of the as-prepared Yb3Tm0.05 glass prepared with 2 wt% of PeL particles and of the same composite after heat treatment at (T_g+20 °C) for 17 h and then at 390 °C for 1 h are measured following 2 min of 980 nm illumination and are shown in Fig. 13b: the as-prepared sample reaches the 0.3 mcd/m^2 limit within 14 min while the heat treated glass emits green afterglow above 0.3 mcd/m^2 for 8 min. Under IR illumination, the phosphor is charged by the UC emission bands that overlaps with the thermoluminescence excitation spectrum. In case of the as-prepared glass, this includes only the 475 nm emission from the $^1G_4$ level whereas the heat treated glass also exhibits emission from the $^1D_2$ level (around 361 nm and 450 nm) and the $^1I_6$ level (around 346 nm) (Fig. 9). Hence if only the overlap between the UC emission and the thermoluminescence excitation spectrum is considered, the shorter afterglow time of the heat treated sample is quite unexpected. However, the difference in scattering properties

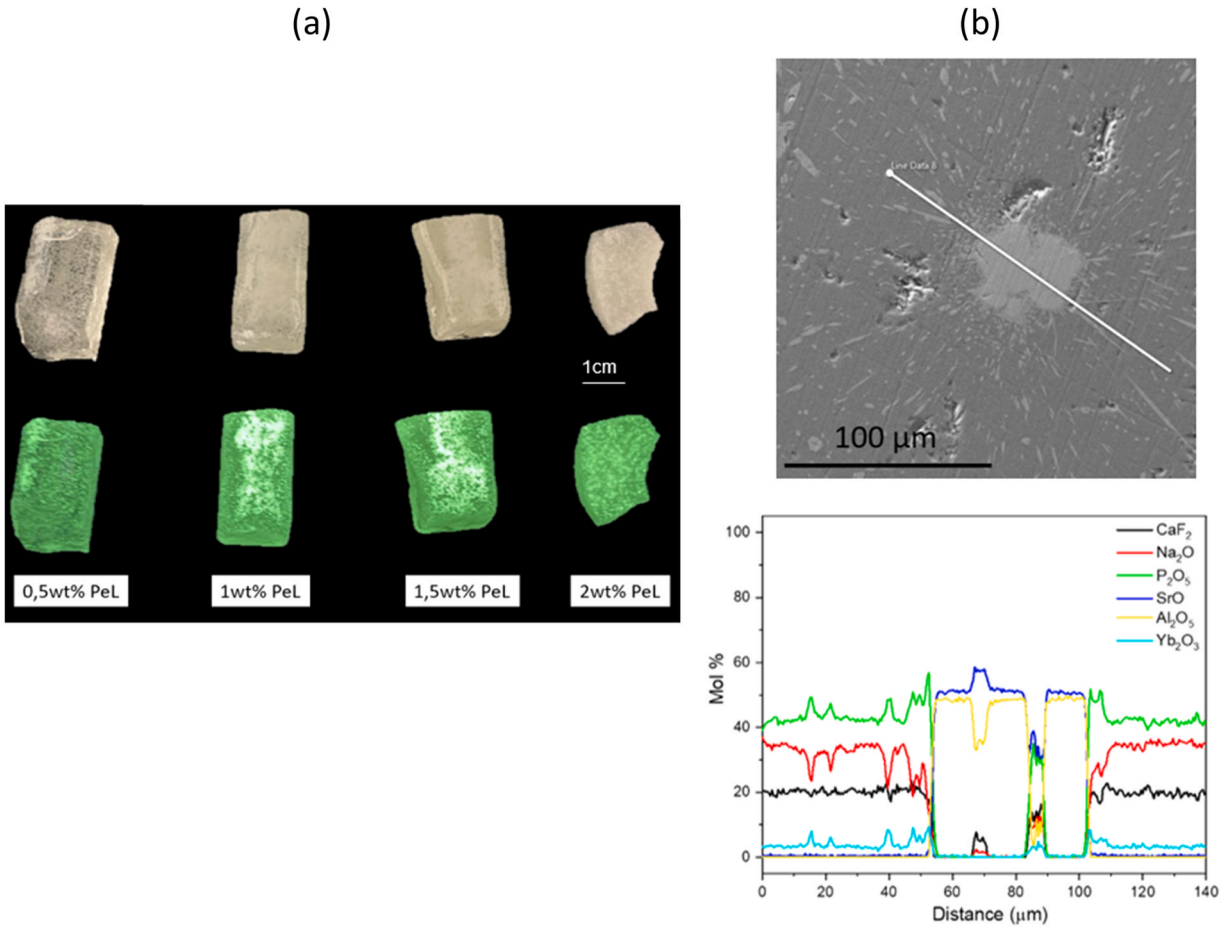

Fig. 11. (a) Picture in daylight and after stopping the UV of the Yb3Tm0.05 glasses prepared with different wt% of PeL particles; (b) SEM images of a PeL particle found at the surface of the polished Yb3Tm0.05 glass prepared with 2 wt% of PeL particles with corresponding composition analysis.

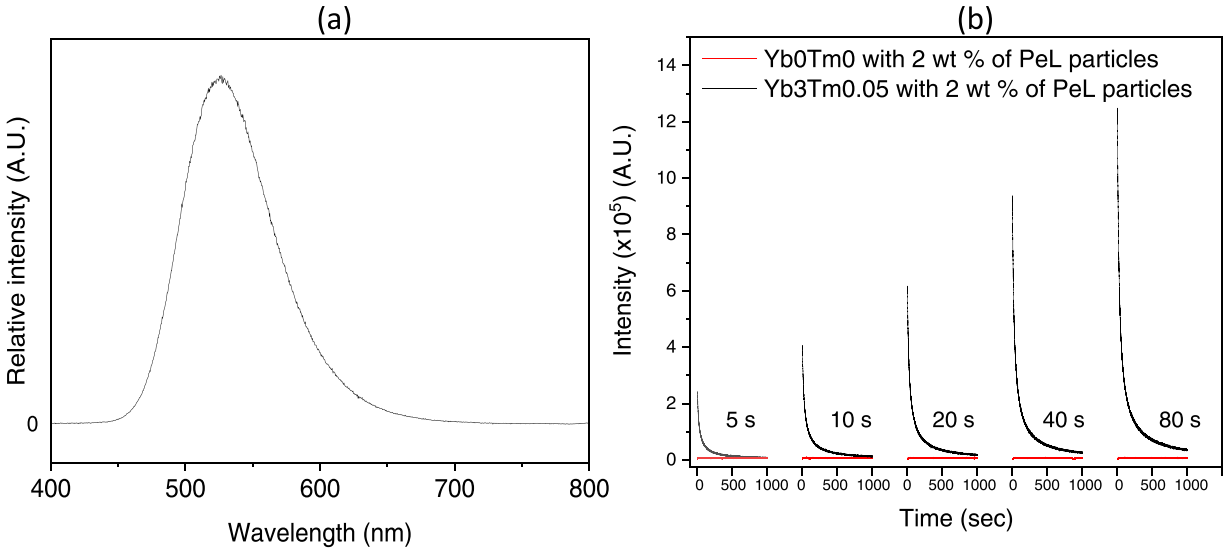

Fig. 12. (a) PeL spectra of the glass prepared with 2 wt% of PeL particles, taken as an example, after 980 nm charging for 2 min. The PeL spectra were recorded 15 s after stopping the irradiation; (b) Integrated afterglow intensity of the Yb3Tm0.05 glass prepared with 2 wt% of PeL particles and from the Yb0Tm0 glass containing 2 wt% of PeL particles as a function of illumination time with 980 nm illumination.

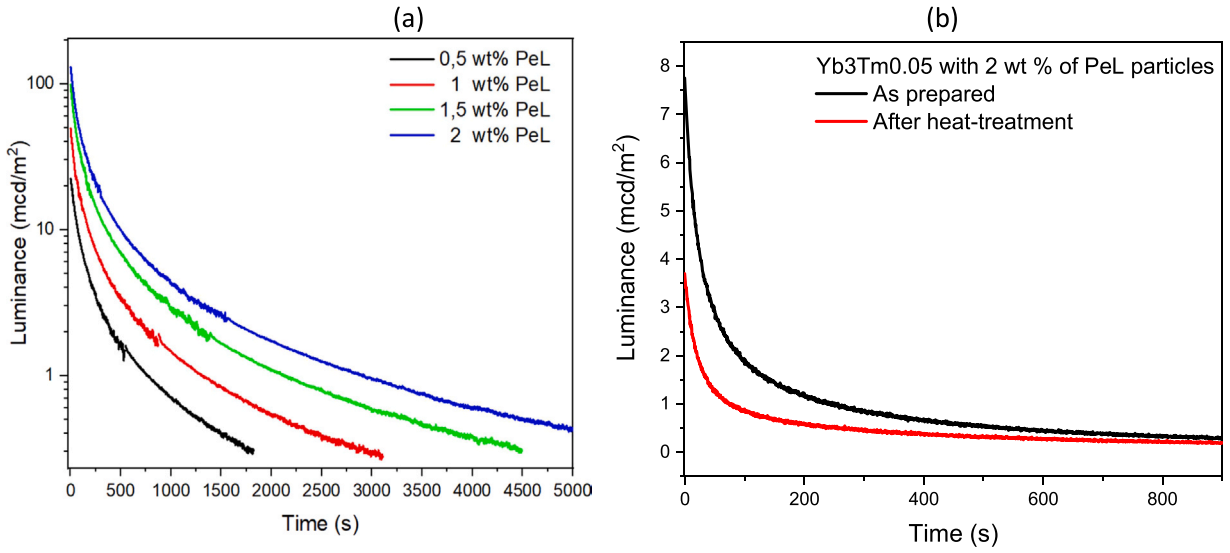

Fig. 13. (a) Decay curves obtained from the Yb3Tm0.05 glasses prepared with different wt% of PeL particles after 254 nm charging. (b) Decay curves obtained from the Yb3Tm0.05 glass prepared with 2 wt% of PeL particles, prior to and after heat treatment at (T_g+20 °C) for 17 h and then at 390 °C for 1 h, after two minutes of 980 nm charging.

and the slight difference in the shape of the measured crystals should also be taken into account when comparing the two samples.

Although the afterglow intensity after 980 nm illumination is much lower compared to the one obtained after 254 nm illumination, it should be stressed that the infrared excitation is here considered as an additional excitation route rather than an alternative to direct blue or UV excitation of the PeL particles. These results clearly demonstrate that the newly developed Yb^{3+} Tm^{3+} co-doped glasses exhibit a blue (475 nm) or blue and UV (346, 361 and 450 nm) UC emission that is intense enough to charge the green PeL particles.

4. Conclusion

In summary, we demonstrated that oxyfluorophosphate glasses in the $NaPO_3$-CaF_2 system can be prepared with intense UC emission upon excitation at 980 nm by adding Yb^{3+} and Tm^{3+}. The addition of Yb^{3+} enhances the UC emission of Tm^{3+} due to energy transfer between Yb^{3+} and Tm^{3+}. A heat treatment of the glasses leads to the precipitation of CaF_2 crystals which contain Yb^{3+} and Tm^{3+}, increasing the intensity of the UC emission only in the glasses prepared with 1 mol% of Yb_2O_3, as reverse energy transfer from Tm^{3+} to Yb^{3+} is observed from the glasses prepared with larger Yb_2O_3 content. Despite the decrease in UC emission intensity from the $^1G_4$ level (475 nm), the samples with a larger Yb_2O_3 content exhibit also UV (346, 361 nm) and blue (450 nm) emissions from the $^1I_6$ and $^1D_2$ levels which overlap well with the excitation spectrum of the PeL $SrAl_2O_4$:Eu,Dy particles. It is shown that the direct doping method used to prepare the oxyfluorosphate glass with the PeL particles (composite) needs to be modified to avoid not only the decomposition of the PeL particles occurring during the glass melting but also the extended fluorine evaporation which leads to a noticeable decrease in the intensity of the UC emission. Here, we clearly show that the intensity of the UC emission from the most promising glass is intense enough to charge the PeL $SrAl_2O_4$:Eu^{2+},Dy^{3+} particles leading to green PeL after exposure to 980 nm light, confirming that the newly designed composites are promising materials for infrared-chargeable PeL materials.

CRediT authorship contribution statement

L.P. conceived and designed this work. N.G.A. and L.P. prepared and characterized the glasses. S.V., H.B. and M.L. carried out the spectroscopic measurement of the materials with persistent luminescence while P.S. and D.V.D.H. focused on the experiment to distinguish between charging by up-conversion or optically stimulated luminescence-related phenomena. All authors discussed the results and contributed to the writing of the manuscript.

Data Availability

Data will be made available on request.

Declaration of Competing Interest

The authors declare that they have no known competing financial interests or personal relationships that could have appeared to influence the work reported in this paper.

Acknowledgements

This work was supported by Academy of Finland [Flagship Programme, Photonics Research and Innovation PREIN-320165 and Academy Project −326418]. PS and DVDH acknowledge the financial support from the UGent Special Research Fund (BOF) (project ENCLOSE) and from the FWO (project G0F9322N). We would like to thank Philippe Volckaert from Bureau Veritas Laboratoires (Pessac, France) for the EPMA measurement and Dr. Rolindes Balda from University of the Basque Country (Spain) for the measurement of the spectroscopic properties obtained using 791 nm excitation. This work made use of Tampere Microscopy Center facilities at Tampere University.

References

[1] R.W. Boyd, J.H. Heebner, Sensitive disk resonator photonic biosensor, Appl. Optics 40 (2001) 5742.
[2] O. Graydon, W.H. Loh, R.I. Laming, L. Dong, Triple-frequency operation of an Er-doped twincore fiber loop laser, IEEE Photonics Technol. Lett. 8 (1996) 63–65.
[3] A. Shalav, B.S. Richards, M.A. Green, Luminescent layers for enhanced silicon solar cell performance: up-conversion, Sol. Energy Mater. Sol. Cells 91 (2007) 829–842.
[4] H. Lian, Z. Hou, M. Shang, D. Geng, Y. Zhang, J. Lin, Rare earth ions doped phosphors for improving efficiencies of solar cells, Energy 57 (2013) 270–283.
[5] D. Nakauchi, G. Okada, M. Koshimizu, T. Yanagida, Storage luminescence and scintillation properties of Eu-doped $SrAl_2O_4$ crystals, J. Lumin. 176 (2016) 342–346.
[6] F. Auzel, Materials and devices using double-pumped-phosphors with energy transfer, Proc. IEEE 61 (1973) 758.

[7] V. Venkatramu, P. Babu, C.K. Jayasankar, Fluorescence properties of Eu^{3+} ions doped borate and fluoroborate glasses containing lithium, zinc and lead, Spectrochim. Acta, Part A 63 (2006) 276–281.

[8] W.J. Miniscalco, Erbium-doped glasses for fiber amplifiers at 1500 nm, J. Light. Technol. 9 (1991) 234–250.

[9] J.H. Campbell, T.I. Suratwala, Nd-doped phosphate glasses for high-energy/high-peak-power lasers, J. Non-Cryst. Solids 263–364 (2000) 318–341.

[10] T.I. Suratwala, R.A. Steele, G.D. Wilke, J.H. Campbell, K. Takeuchi, Effects of OH content, water vapor pressure, and temperature on sub-critical crack growth in phosphate glass, J. Non-Cryst. Solids 263–264 (2000) 213–227.

[11] B. Jacquier, C. Linare's, R. Mahiou, J.L. Adam, J. Lucas, Efficient blue upconversion in Tm^{3+} and Pr^{3+} doped BIGaZYbTZr glasses, J. Lumin. 60–61 (1994) 175–178.

[12] M. Poulain, Overview of crystallization in fluoride glasses, J. Non-Cryst. Solids 140 (1992) 1–9.

[13] S. Cui, J. Massera, M. Lastusaari, L. Hupa, L. Petit, Novel fluorophosphates glasses and glass-ceramics, J. Non-Cryst. Solids 445–446 (2016) 40–44.

[14] Y. Wang, J. Ohwaki, New transparent vitroceramics codoped with Er^{3+} and Yb^{3+} for efficient frequency upconversion, Appl. Phys. Lett. 63 (1993) 3268.

[15] P.A. Tick, N.F. Borrelli, L.K. Cornelius, M.A. Newhouse, Transparent glass ceramics for 1300 nm amplifier applications, J. Appl. Phys. 78 (1995) 6367.

[16] F. Leon-Luis, J. Abreu-Afonso, J. Pena-Martınez, J. Mendez-Ramos, A.C. Yanes, J. del-Castillo, V.D. Rodrıguez, Up-conversion and colour tunability in Yb^{3+}–Er^{3+}–Tm^{3+} co-doped transparent nano-glass-ceramics, J. Alloy. Compd. 479 (2009) 557–560.

[17] J. Zhang, D. He, Z. Duan, L. Zhang, S. Dai, L. Hu, Mechanisms and concentrations dependence of up-conversion luminescence in Tm^{3+}/Yb^{3+} codoped oxyfluoride glass-ceramics, Phys. Lett. A 337 (2005) 480–486.

[18] N. Hemono, G. Pierre, F. Munoz, A. de Pablos-Martın, M.J. Pascual, A. Duran, Processing of transparent glass-ceramics by nanocrystallisation of LaF_3, J. Eur. Ceram. Soc. 29 (2009) 2915–2920.

[19] J. Xing, L. Liu, F. Shang, G. Chen, Preparation, structure and temperature dependence of spectral properties of Yb^{3+}/Er^{3+} doped $Sr_5(PO_4)_3F$ transparent glass ceramics, J. Alloy. Compd. 884 (2021) 161018.

[20] A. Szczodra, A. Mardoukhi, M. Hokka, N.G. Boetti, L. Petit, Fluorine losses in Er^{3+} oxyfluoride phosphate glasses and glass-ceramics, J. Alloy. Compd. 797 (2019) 797–803.

[21] L. Hu, P. Wang, M. Zhao, L. Liu, L. Zhou, B. Li, F.H. Albaqami, A.M. El-Toni, X. Li, Y. Xie, X. Sun, F. Zhang, Near-infrared rechargeable "optical battery" implant for irradiation-free photodynamic therapy, Biomaterials 163 (2018) 154–162.

[22] M.R. Henderson, B.C. Gibson, H. Ebendorff-Heidepriem, K. Kuan, V.S. Afshar, J.O. Orwa, I. Aharonovich, S. Tomljenovic-Hanic, A.D. Greentree, S. Prawer, T.M. Monro, Diamond in tellurite glass: a new medium for quantum information, Adv. Mater. 23 (2011) 2806–2810.

[23] H. Zhong, G. Chen, L. Yao, J. Wang, Y. Yang, R. Zhang, The white light emission properties of Tm^{3+}/Tb^{3+}/Sm^{3+} triply doped SrO–ZnO–P_2O_5 glass, J. Non-Cryst. Solids 427 (2015) 10–15.

[24] A.E. Ersundu, G. Karaduman, M. Çelikbilek, N. Solak, S. Aydın, Effect of rare-earth dopants on the thermal behavior of tungsten–tellurite glasses, J. Alloy. Compd. 508 (2010) 266–272.

[25] A. Nommeots-Nomm, N.G. Boetti, T. Salminen, J. Massera, M. Hokka, L. Petit, Luminescence of Er^{3+} doped oxyfluoride phosphate glasses and glass-ceramics, J. Alloy. Compd. 751 (2018) 224–230.

[26] N. Ojha, I. Dmitrieva, W. Blanc, L. Petit, Tailoring the glass composition to increase the thermal stability without impacting the crystallization behavior of oxyfluorophosphate glass, Ceramics 4 (2021) 148–159.

[27] I. Konidakis, C.P.E. Varsamis, E.I. Kamitsos, D. Möncke, D. Ehrt, Structure and properties of mixed strontium–manganese metaphosphate glasses, J. Phys. Chem. C. 114 (2010) 9125–9138.

[28] R.K. Brow, D.R. Tallant, S.T. Myers, C.C. Phifer, The short-range structure of zinc polyphosphate glass, J. Non-Cryst. Solids 191 (1995) 45–55.

[29] H. Gao, T. Tan, D. Wang, Effect of composition on the release kinetics of phosphate controlled release glasses in aqueous medium, J. Control. Release 96 (2004) 21–28.

[30] B. Qian, X. Liang, S. Yang, S. He, L. Gao, Effects of lanthanum addition on the structure and properties of iron phosphate glasses, J. Mol. Struct. 1027 (2012) 31–35.

[31] R. Koch, W.A. Clarkson, D.C. Hanna, S. Jiang, M.J. Myers, D. Rhonehouse, S.J. Hamlin, U. Griebner, H. Schonnagel, Efficient room temperature cw Yb:glass laser pumped by a 946 nm Nd:YAG laser, Opt. Commun. 134 (1997) 175–178.

[32] A. Kar, S. Kundu, A. Patra, Lanthanide-doped nanocrystals: strategies for improving the efficiency of upconversion emission and their physical understanding, ChemPhysChem 16 (2015) 505–521.

[33] M.C. Falconi, D. Laneve, V. Portosi, S. Taccheo, F. Prudenzano, Design of a Multi-wavelength Fiber Laser Based on Tm:Er:Yb:Ho Co-Doped Germanate Glass, J Light Technol 38 (2020), pp. 2406–2413.

[34] N. Ojha, A. Szczodra, N.G. Boetti, J. Massera, L. Petit, Nucleation and growth behavior of Er^{3+} doped oxyfluorophosphate glasses, RSC Adv. 10 (2020) 25703–25716.

[35] J.J. Velázquez, R. Balda, J. Fernández, G. Gorni, M. Sedano, A. Durán, D. Galusek, M.J. Pascual, Structural and optical properties in Tm^{3+}/Tm^{3+}–Yb^{3+} doped $NaLuF_4$ glass-ceramics, Int. J. Appl. Glass Sci. 12 (2021) 485.

[36] J.J. Velázquez, A.C. Yanes, J. del Castillo, J. Méndez-Ramos, V.D. Rodríguez, Optical properties of Ho^{3+}-Yb^{3+} co-doped nanostructured SiO_2-LaF_3 glass-ceramics prepared by sol-gel method, Phys. Status Solidi 204 (6) (2007) 1762–1768.

[37] W. Wang, J. Tian, J. Dong, Y. Xue, D. Hu, W. Hou, H. Tang, Q. Wang, X. Xu, J. Xu, Growth, spectroscopic properties and up-conversion of Yb, Pr co-doped CaF_2 crystals, J. Lumin. 233 (2021) 117931.

[38] D. Chen, Y. Wang, Y. Yu, P. Huang, Intense ultraviolet upconversion luminescence from Tm^{3+}/Yb^{3+}: β-YF_3 nanocrystals embedded glass ceramic, Appl. Phys. Lett. 91 (2007) 051920.

[39] A.J.J. Bos, R.M. van Duijvenvoorde, E. van der Kolk, W. Drozdowski, P. Dorenbos, Thermoluminescence excitation spectroscopy: a versatile technique to study persistent luminescence phosphors, J. Lumin. 131 (2011) 1465–1471.

[40] N. Ojha, M. Tuomisto, M. Lastusaari, L. Petit, Phosphate glasses with blue persistent luminescence prepared using the direct doping method, Opt. Mater. 87 (2019) 151–156.

[41] P. Roldán Del Cerro, T. Salminen, M. Lastusaari, L. Petit, Persistent luminescent borosilicate glasses using direct particles doping method, Scr. Mater. 151 (2018) 38–41.

[42] N. Ojha, T. Laihinen, T. Salminen, M. Lastusaari, L. Petit, Influence of the phosphate glass melt on the corrosion of functional particles occurring during the preparation of glass-ceramics, Ceram. Int. 44 (2018) 11807–11811.

[43] N. Ojha, H. Nguyen, T. Laihinen, T. Salminen, M. Lastusaari, L. Petit, Decomposition of persistent luminescent microparticles in corrosive phosphate glass melt, Corros. Sci. 135 (2018) 207–214.

[44] A. Szczodra, L. Kuusela, I. Norrbo, A. Mardoukhi, M. Hokka, M. Lastusaari, L. Petit, Successful preparation of fluorine containing glasses with persistent luminescence using the direct doping method, J. Alloy. Compd. 787 (2019) 1260–1264.

[45] J. Massera, M. Gaussiran, P. Gluchowski, M. Lastusaari, L. Hupa, L. Petit, Processing and characterization of phosphate glasses containing $CaAl_2O_4$:Eu^{2+},Nd^{3+} and $SrAl_2O_4$:Eu^{2+},Dy^{3+} microparticles, J. Eur. Ceram. Soc. 35 (2015) 3863–3871.

[46] V. Lahti, N. Ojha, S. Vuori, M. Lastusaari, L. Petit, Preparation of glass-based composites with green upconversion and persistent luminescence using modified direct doping method, Mater. Chem. Phys. 274 (2021) 125164.

[47] A.J.J. Bos, R.M. van Duijvenvoorde, E. van der Kolk, W. Drozdowski, P. Dorenbos, Thermoluminescence excitation spectroscopy: a versatile technique to study persistent luminescence phosphors, J. Lumin. 131 (2011) 1465–1471.

[48] L. Yuan, Y. Jin, Y. Su, H. Wu, Y. Hu, S. Yang, Optically stimulated luminescence phosphors: principles, applications, and prospect, Laser Photonics Rev. 14 (2020) 2000123.

[49] D. Van der Heggen, D.R. Cooper, M. Tesson, J.J. Joos, J. Seuntjens, J.A. Capobianco, P.F. Smet, Optically Stimulated Nanodosimeters with High Storage Capacity, Nanomaterials 9 (2019) 1127.

[50] J. Xu, D. Murata, J. Ueda, B. Viana, S. Tanabe, Toward rechargeable persistent luminescence for the first and third biological windows via Persistent energy transfer and electron trap redistribution, Inorg. Chem. 57 (2018) 5194–5203.

[51] S.K. Sharma, D. Gourier, E. Teston, D. Scherman, C. Richard, B. Viana, Persistent luminescence induced by near infra-red photostimulation in chromium-doped zinc gallate for in vivo optical imaging, Opt. Mater. 3 (2017) 51–58.

[52] D. Van der Heggen, D. Vandenberghe, N.K. Moayed, J. De Grave, P.F. Smet, J.J. Joos, The almost hidden role of deep traps when measuring afterglow and thermoluminescence of persistent phosphors, J. Lumin. 226 (2020) 117496.

[53] Deutsche Norm. Phosphorescent Pigments and Products – Part 1: Measurement and Marking at the Producer. 2009, p DIN 67510–1:2009–11.